12

Energetic-particle environments in the solar system

NORBERT KRUPP

Energetic particles in our heliosphere are key in the understanding of the evolution and the current status of our solar system. The energy distributions of ions and electrons are widely used to understand acceleration phenomena in the heliosphere and in the vicinity of planets and moons. Knowing the energy spectra of those particles can tremendously help in the characterization of plasma sources and sinks of many different environments in the Milky Way and beyond. The knowledge of those energetic particle distributions in fact is essential in many fundamental plasma physics problems. They are a very nice tool to investigate acceleration mechanisms, geochemistry and solar-system evolution, atmospheric composition and solar-system evolution, and last but not least energetic particles are important in studying the configuration and dynamics of planetary magnetospheres and the interaction of magnetospheric plasma with their moons, rings, neutral gas, or dust clouds.

Energetic particles in the energy range between 1 eV to 10^{20} eV can be found everywhere in our solar system as sketched in Fig. 12.1. Their sources can be either outside our solar system from galactic or extra-galactic interstellar space or inside our solar system from the Sun or the planets or created in various acceleration processes in interplanetary space or inside planetary magnetospheres, i.e., at interplanetary shocks, corotating interaction regions, planetary bow shocks or at the termination shock of the heliosphere. Types of energetic particles range from electrons to charged atoms and molecules to neutral atoms and molecules as well as dust particles. Figure 12.2 shows the particle intensity versus energy spectra of various types of energetic particles (left) and for cosmic rays (right).

This chapter focuses on the description of charged energetic particle populations from the Sun and particle distributions inside planetary magnetospheres (including galactic cosmic rays (GCRs) as a potential source of charged particles in planetary radiation belts). Energetic particles from acceleration processes at shocks are reviewed in Ch. 7 of Vol. II.

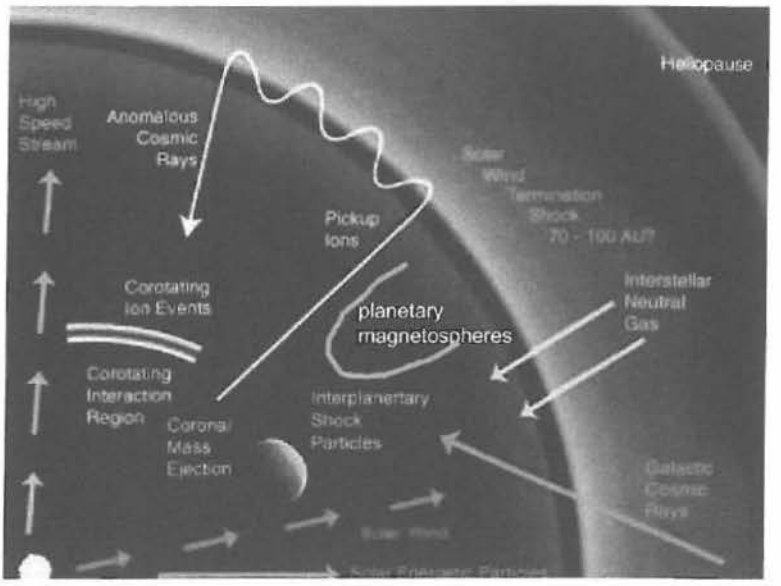

Fig. 12.1 Sources of energetic particles in the heliosphere. (Adapted from www.issibern.ch/teams/Suprat.)

In order to set the scene for later sections and without going into much detail we introduce the motion of charged particles in a magnetic field. For further details and equation derivations the reader is referred to books like Roederer (1970) or Walt (1994). A excellent text used for this chapter is Kallenbach *et al.* (2006).

Starting from the fundamental equation of charged particle motion the Lorentz force $\vec{F}$ is given by

$$\vec{F} = \frac{d\vec{p}}{dt} = q(\vec{v} \times \vec{B} + \vec{E}), \tag{12.1}$$

with $\vec{v}$, $\vec{p}$, $\vec{B}$, $\vec{E}$ being the particle velocity, particle momentum, magnetic field, and electric field vectors, and q being the elementary charge. In a uniform magnetic field the momentum component parallel to the magnetic field is constant and its derivative is equal to zero. Centrifugal force balances the Lorentz force and the resulting motion of the particle is a circle when projected into a plane perpendicular to the magnetic field direction with the cyclotron or gyroradius r_G given by

$$r_G = \frac{mv_\perp}{|q|B} = \frac{v_\perp}{|\omega_G|}, \tag{12.2}$$

where ω_G is the gyrofrequency. The gyromotion direction is given by the sign of the charge of the particle. In addition to the motion perpendicular to the magnetic field the particle can also move parallel to it. The pitch angle $\alpha = \tan^{-1}(\frac{v_\perp}{v_\parallel})$ is the

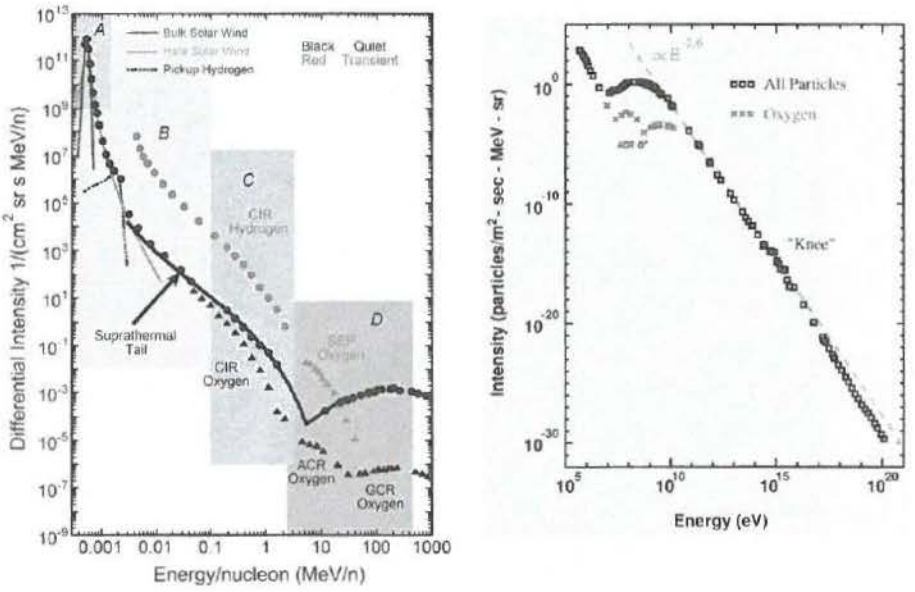

Fig. 12.2 Energy spectra of energetic particles in the heliosphere (left) and for cosmic rays (right). The curves illustrate the energy spectra during quiet time and disturbed solar wind conditions. The dots and triangles represent the suprathermal part of the spectrum and the particles accelerated at corotating interaction regions (CIRs), galactic cosmic rays (GCRs), and the anomalous cosmic rays (ACRs) together with Solar Energetic Particles (SEPs). The right figure shows the high-energy part of the GCR energy spectrum to TeV energies. Note the characteristic peak at about 10 MeV and the $E^{-2.6}$power-law dependence for energies above the peak. (Figure adapted from Ch. 3 in Vol. II.)

angle between the particle velocity vector and the direction of the magnetic field. The gyration creates a current I, a magnetic flux ϕ, and a magnetic moment μ.

The magnetic moment is defined as

$$\vec{\mu_G} = \frac{mv_\perp^2}{2B^2}\vec{B}|\mu| = \frac{W_\perp}{B}. \tag{12.3}$$

where $W_\perp$ is the particle energy perpendicular to the magnetic field. The first adiabatic invariant of a particle is defined as μ = constant, which means that a charged particle moving in a changing magnetic field conserves its magnetic moment and, as a consequence, changes its energy component perpendicular to the magnetic field.

The second adiabatic invariant J of a charged particle describes the periodic parallel motion or bounce motion back and forth along the magnetic field:

$$J = \oint mv_\parallel ds = \frac{v_\perp d\alpha}{\omega_G}. \tag{12.4}$$

From μ = constant it follows that a charged particle with a pitch angle α_1 in a magnetic field B_1 moves up and down the field line until it reaches a point (mirror point) where the magnetic field is $B_m = B_1/\sin\alpha_1^2$ and is reflected by the related mirror force $-\mu\nabla B$.

Finally the third adiabatic invariant for a charged particle describes approximately the magnetic flux conservation enclosed by the full drift motion around a planet for example.

$$\phi = \frac{2\pi m}{q^2} M = \text{constant}, \tag{12.5}$$

with M being the magnetic moment of the enclosed magnetic field. For details see Northrop (1963).

The presence of a uniform magnetic and electric field perpendicular to each other results in a drift of particles perpendicular to $\vec{B}$ and $\vec{E}$:

$$\vec{V}_E = \frac{\vec{E} \times \vec{B}}{B^2}. \tag{12.6}$$

In the presence of an inhomogeneous magnetic field the gradient in B and the curvature of the field lines cause deviations which can be described by the gradient drift

$$\vec{V}_G = \frac{m v_\perp^2}{2q B^3}(\vec{B} \times \nabla B) \tag{12.7}$$

and the curvature drift

$$\vec{V}_C = \frac{m v_\parallel^2}{q B^3}(\vec{B} \times \nabla B). \tag{12.8}$$

The total drift velocity of a particle is a combination of all three:

$$\vec{V}_\perp = \vec{V}_E + \vec{V}_G + \vec{V}_C = \frac{\vec{E} \times \vec{B}}{B^2} + \frac{m}{q B^3}\left(\frac{v_\perp^2}{2} + v_\parallel^2\right)\vec{B} \times \nabla B. \tag{12.9}$$

As an example of drift values the bounce-averaged drift velocity in Saturn's magnetosphere is shown together with equatorial gyroradius and bounce period as a function of dipole L in Fig. 12.3.

The detection of energetic charged particles goes back to the pioneers in space instrumentation like James van Allen in the late 1950s, when the first rocket-based "Geiger counters" measured huge intensity increases and dropouts at several thousand kilometers altitude above the Earth. The historic discovery of the Earth's radiation belts was made by measuring the charged particle environment of the Earth. In the beginning, relatively simple counters were used, followed by more advanced semiconductor detector devices and electrostatic analyzers. A real breakthrough was the possibility to distinguish between different energies, different

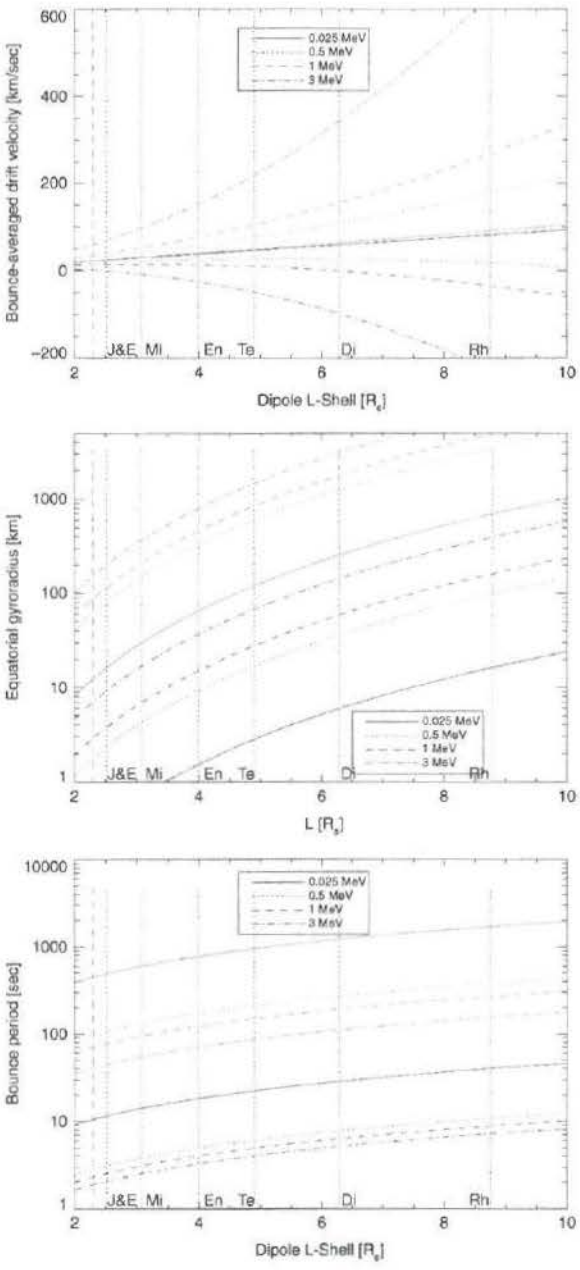

Fig. 12.3 Top: bounce-averaged drift velocities at Saturn as a function of energy and L-shell (lower four curves for electrons and upper four curves for ions). All values are for equatorial particles (90 degree pitch angle) assuming rigid corotation in an inertial, Saturn-centered coordinate system. Middle: same plot for the gyroradius of equatorial electrons and ions. Bottom: bounce period of electrons and ions with a pitch angle of 45 degrees. In all panels, the location of the various icy moon L-shells are indicated with dotted lines. The dashed line indicates the L-shell of the main ring's outer edge. (From Roussos, 2008.)

species, and different directions using combinations of so called time-of-flight systems and post-acceleration subunits. Today's technology makes it possible to "visualize" the invisible particle environment. Particle detectors with imaging capabilities measure charged and even neutral particles at energies between eV and GeV. A nicely summarized description of particle detector types can be found in Gloeckler (2010).

12.1 Energetic particles from the Sun

The first detection of solar energetic particles goes back to 1946 when Scott Forbush related the source of high-energy-particle intensity increases to the Sun and not to cosmic rays (Forbush, 1946). Since then solar energetic particles have been measured in a wide range of energies between keV and GeV. They are observed on time scales between several hours up to several days. Their intensities increase above average by several orders of magnitude. Details are found in Kallenrode (2003), Reames *et al.* (2013), Reames (2013), Kahler (2013a,b), and Kahler and Vourlidas (2013). It is currently accepted that the occurrence of energetic particles is directly related to either Solar Flares or to Coronal Mass Ejections (CMEs). The ultimate energy source of those particles is the magnetic energy of the Sun. As nicely illustrated in Fig. 12.4 from Kallenrode (2003), the idea is that an instability triggers a flare or a CME with a number of associated acceleration mechanisms

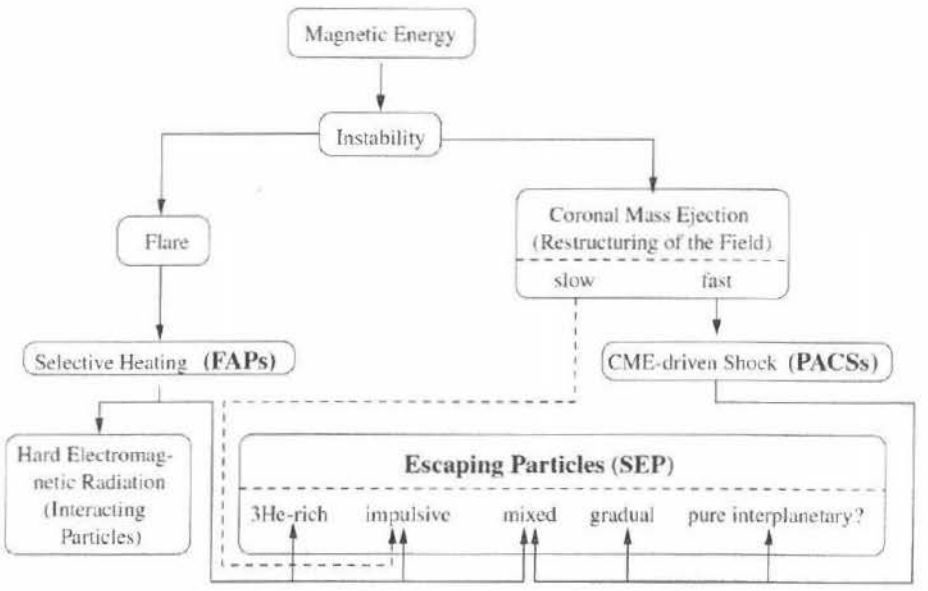

Fig. 12.4 Classification of solar energetic-particle events. (From Kallenrode, 2003.)

and/or compositional variations of Sun material, i.e., enrichment of ^{3}He relative to ^{4}He, etc. For a full description the reader is referred to the original literature starting from Kallenrode (2003) and earlier references therein.

The classification of solar energetic particle events into "^{3}He-rich", "impulsive", and "gradual" is based on a number of parameters such as relative abundance ratios of ^{3}He/^{4}He, H/He, Fe/O to name a few (after Reames, 1995). Solar energetic particle events are also in good correlation to the observation of type II or type III radio bursts on the Sun (Kane *et al.*, 1974).

12.1.1 Energetic particles from Coronal Mass Ejections (CMEs)

Coronal Mass Ejections are events originating at the Sun where particles are trapped in closed magnetic loop structures. Their footpoints are still connected to the Sun's surface and the entire structure is moving outwards. CMEs are well-known features, since their first discovery in the 1970s with coronagraph instruments onboard spacecraft. Data of the LASCO coronagraph, an instrument onboard the ESA/NASA spacecraft SOHO (launched in 1996), could show that CME characteristics vary from event to event. The CMEs move at speeds between 50 km/s and more than 2000 km/s with large angular widths which could cover the entire sky. During CMEs billions of tons of material are ejected.

Figure 12.5 shows the spatial structure of a CME as observed by the LASCO instrument onboard SOHO. It is clearly visible that CMEs consists of three different clearly distinguished spatial regions: a leading edge, a cavity, and a core.

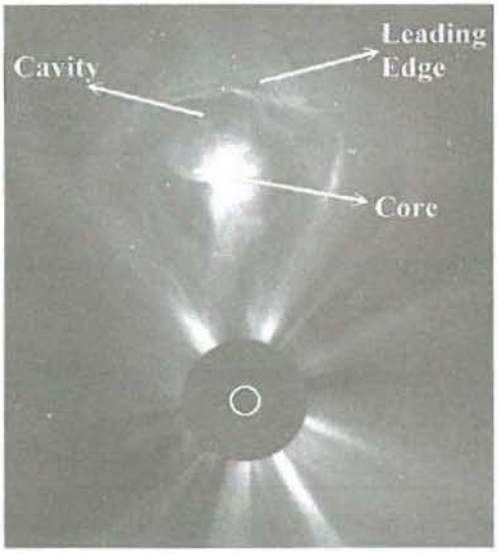

Fig. 12.5 CME spatial structures. (From Rodriguez, 2005.)

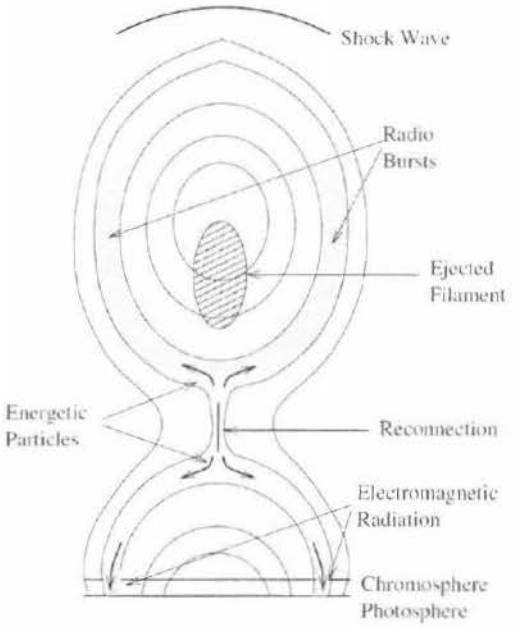

Fig. 12.6 Concepts of particle acceleration in a solar gradual event. (Adapted from Kallenrode, 2003.)

Gradual events are those particles observed in correlation to fast shock waves driven by CMEs in the corona of the Sun or in interplanetary space. The acceleration process itself in those events could be either shock drift acceleration, diffusive shock acceleration (Fermi 1 acceleration) or stochastic acceleration (Fermi 2 acceleration). For further discussion of these processes, the reader is referred to Ch. 7 in Vol. II.

The principal scenario of particle acceleration in those gradual events is sketched in Fig. 12.6 (Kallenrode, 2003). Energetic particles are accelerated close to the magnetic reconnection region where they move bi-directionally along the field lines. As pointed out by Reames *et al.* (2013) the acceleration on the shock wave occurs on open magnetic field lines in contrast to the closed magnetic loop picture.

The intensities of those gradual events observed at different solar longitudes relative to the nose of the shock front are shown in Fig. 12.7. The intensity–time profiles are quite different from each other and depend on the location of the observer relative to the nose of the shock front.

Near the nose of shock front they display a four-stage intensity–time profile as shown in Fig. 12.8 from Reames (2013): onset (velocity-dispersed with highest velocity ions arriving first), plateau (generated Alfvén waves scatter outward streaming particles up to a "streaming limit"), shock peak (enhancement typical for shock acceleration), and reservoir (slow time decay of intensities). Only the large events create high-energy particles.

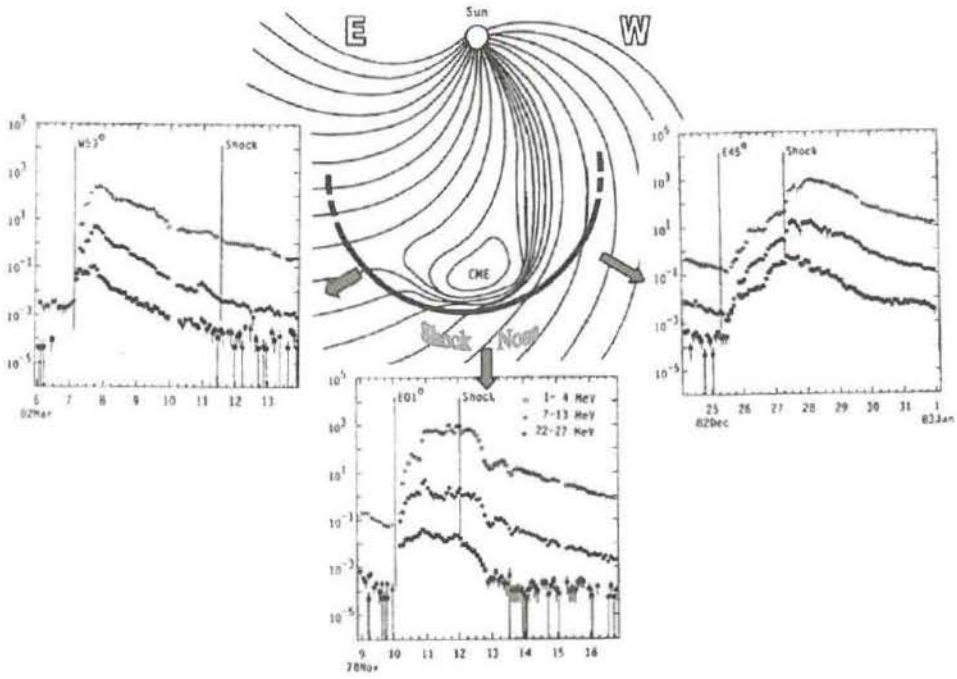

Fig. 12.7 Intensity–time plots of particle fluxes ejected from three different solar longitudes with respect to the nose of the shock front. (From Reames, 2013.)

12.1.2 Flares

Impulsive events originate in impulsive jets or flares on the Sun and are observed in correlation with type III radio bursts from outward streaming electrons with energies of about 40 keV (Reames, 2013). Resonant stochastic acceleration caused by magnetic reconnection additionally can also enhance the ^{3}He/^{4}He- and Fe/O-ratio. Figure 12.9 illustrates the scenario.

12.2 Energetic particles in planetary magnetospheres

Planetary magnetospheres represent huge and unique plasma laboratories with sources and sinks of neutral and charged particles in partly rapidly rotating magnetic fields. As described in the introduction section of this chapter the particles in dipole-like magnetic fields gyrate, bounce, and drift in those environments. The adiabatic motion of particles in a rotating magnetosphere is mathematically described in detail by Northrop and Birmingham (1982) and Roederer (1970). The understanding and characterization of transport and motion of those particles are key to understanding astrophysical phenomena in general.

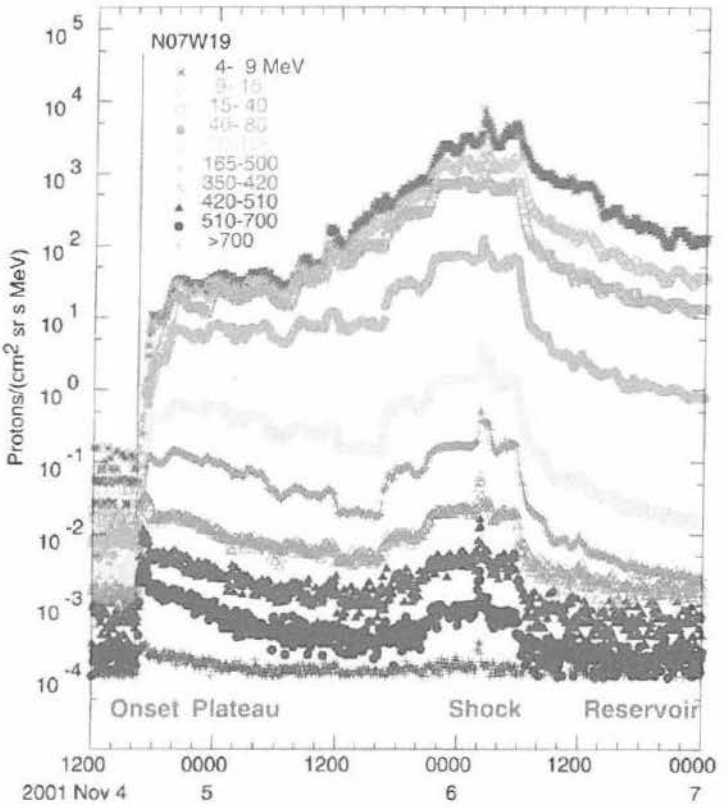

Fig. 12.8 The four phases of a large gradual CME event compared to energy-dependent energetic particle fluxes. This event was observed by NOAA/GOES spacecraft at 1 AU. Different gray shades indicate the intensities of protons for different energies. (From Reames, 2013.)

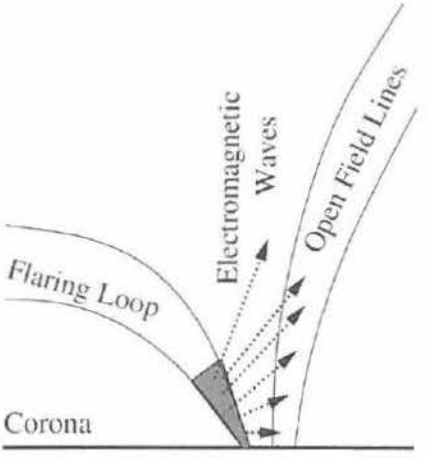

Fig. 12.9 Concept of particle acceleration in an impulsive flare. (Adapted from Kallenrode, 2003.)

Energetic particles are found in planetary magnetospheres in their radiation belts where they are trapped in a strong, basically dipolar magnetic field, bouncing back and forth between the northern and southern hemispheres. Correlated with the high energy and high intensities are radio emissions up to synchrotron radiation when relativistic MeV electrons are present. Energetic particles are also present in the magnetodisk and/or magnetotail regions of planetary magnetospheres where they bounce and drift around the planet. In the Jovian and Saturnian magnetosphere, i.e., the keV–MeV particle population start as neutral particles from their sources Io or Enceladus, get charged by solar UV and are transported radially outwards through the centrifugal forces in the rapidly rotating magnetic fields of the planets. Several hundred kg/s of heavy ions are released into the magnetospheres. As a consequence the magnetic field lines mass-loaded with this material stretch significantly predominantly in the equatorial plane into a magnetodisk configuration until the magnetic stress is too strong and reconnection occurs. Reconnection in the magnetotail, wave–particle interactions, and radial inward diffusion are prime candidates of processes to accelerate those particles from eV to MeV energies.

Energetic particles also play a major role to study planetary aurorae and other high-latitude polar magnetospheric processes. As an example it should be mentioned that hundreds of keV electrons accelerated into Jupiter's atmosphere are mainly responsible for the main auroral oval at Jupiter.

Particle sources can be either the atmosphere or ionosphere of the planet itself, or the sources can be deep inside the magnetospheres as in the cases for Jupiter and Saturn with the moons Io and Enceladus, respectively, or they can be outside the magnetospheres (solar wind or GCRs), being trapped and/or accelerated inside the magnetosphere. Particles are accelerated, at least partially, in these processes. It is currently believed that most of the energetic particles in the outer planet magnetospheres gain their energies up to MeV in the outer magnetosphere. From phase-space density calculations (under conservation of first and second adiabatic invariant) it is currently accepted that most of the particles in the keV–MeV range observed in the middle to inner magnetosphere are diffusing radially inward, gaining energy on the stronger magnetic field. However, especially in the case of Saturn, the inner icy moons orbiting the planet prevent this radially inward motion and most of the particles are lost onto the moons. Therefore the charged particle populations of the radiation belts must have another source: galactic cosmic rays (GCRs).

12.2.1 Galactic cosmic rays as sources of radiation belts

It is currently believed that GCRs originate from supernova explosion remnants. The particles are accelerated at the expanding shock fronts. They enter into our

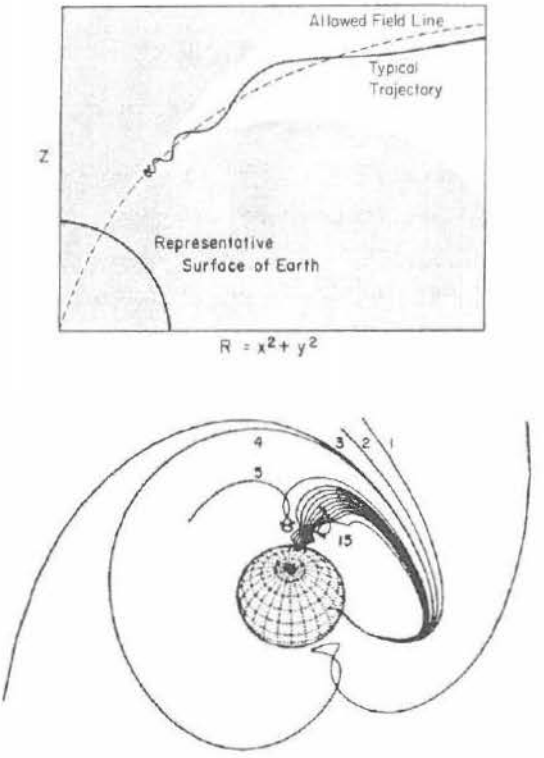

Fig. 12.10 Trajectories of cosmic rays in a planetary dipole field. (Adapted from Smart *et al.*, 2000.)

solar system and can penetrate into planetary magnetospheres on trajectories as shown in Fig. 12.10.

Incoming cosmic rays with GeV energies hit either the atmosphere of a planet or its moons and rings and interact with the material there. As an example Fig. 12.11 shows the simulated spectra of particles produced by 30-GeV protons passing a 10-mm-thick slab of water.

Secondary particles are produced in a wide variety of energies and particle types. For the radiation belts of planetary magnetospheres one of the most important processes is the "cosmic ray albedo neutron decay" (CRAND) in which cosmic rays produce neutrons via knockoff of nucleons in the target material. Most of the neutrons escape from the system, but some of the neutrons decay in the β-process creating protons with lower energy. This is the process to explain MeV protons in inner radiation belts of the Earth or Saturn. The CRAND process is responsible for the peak at about 10 MeV in the energy spectrum of cosmic rays shown in Fig. 12.2. Jupiter's radiation belts are the most intense in the solar system. Figure 12.12 shows

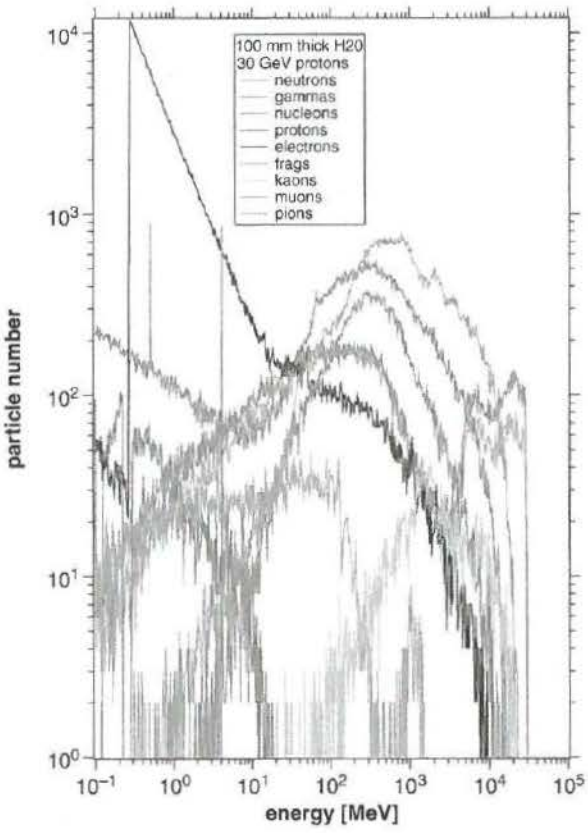

Fig. 12.11 Galactic cosmic-ray spectra for various particle populations. (Diagram provided by D. Haggerty, JHUAPL.) A black and white version of this figure will appear in some formats. For the color version, please refer to the plate section.

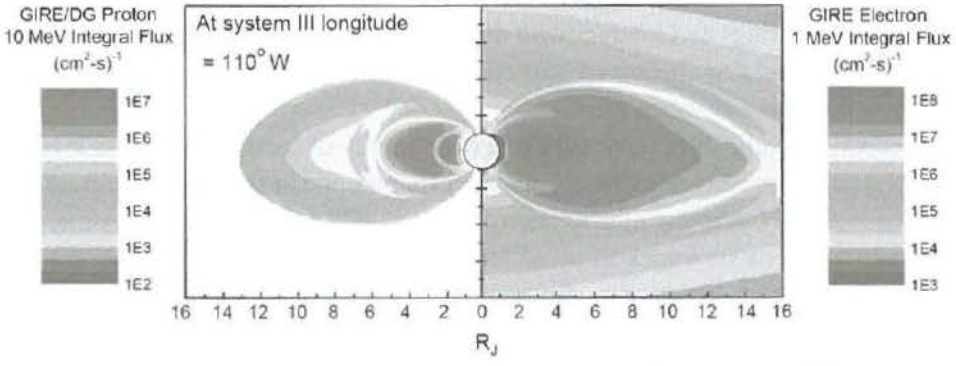

Fig. 12.12 Two-dimensional integral flux distributions for electrons (right section) and protons (left section) at Jupiter based on the Divine-Garrett/GIRE radiation models. (From Paranicas *et al.*, 2009.) A black and white version of this figure will appear in some formats. For the color version, please refer to the plate section.

the modeled integral fluxes of >1 MeV electrons and >10 MeV protons in Jupiter's radiation belts.

MeV electrons with high intensities are found out to at least 10–15 Jovian radii. These relativistic electrons can cause damage in electronics of instruments. Therefore the detailed knowledge of their spatial and energy distribution are crucial to investigate for future missions to Jupiter.

12.2.2 Energetic particles as a useful tool to study magnetospheres

Energetic-particle distributions measured inside planetary magnetospheres are very useful tools to investigate plasma parameters of transport and magnetospheric dynamics. Many new findings are related to the analysis of energetic particles which by far are too many to list them all here in this chapter. They range from the discovery of unknown objects such as moons, plumes, rings, ring arcs, neutral clouds, and tori to the determination of transport parameters, electric fields, flow velocities, open–closed field-line boundaries, surface weathering of moons, remote sensing of surfaces, global imaging of magnetospheric dynamics. Below we describe three examples.

12.2.2.1 Moon absorption signatures in energetic-particle intensities and the determination of diffusion coefficients

The absorption signatures of moons in planetary magnetospheres are distinguished into macrosignatures and microsignatures (Paranicas and Cheng, 1997). Macrosignatures are regions of decreased count rates, where such absorptions are always present at all longitudes along the object's orbit with decreased count rates. As an example Fig. 12.13 shows the macrosignatures of energetic ions (caused by the moons Janus, Mimas, Enceladus, Tethys, and Dione in the Kronian magnetosphere). It is clearly visible that along the L-shells of the corresponding moons and at all latitudes covered by the Cassini measurements a significant depletion is observable.

Microsignatures are small-scale absorptions in the particle distributions highly dependent on the relative position of the causing obstacle and the observer onboard a spacecraft. Moons, planetary rings, or ring arc material as well as dust particles orbiting a planet inside its magnetosphere are subject to heavy "bombardment" from energetic charged particles gyrating, bouncing, and drifting on planetary magnetic field lines. When they hit the object they are lost leaving a gap in the distribution function. Owing to diffusion processes this gap in filled up again slowly. Using the diffusion equation from van Allen *et al.* (1980):

$$f = 1 - 0.5[erf(\frac{1 - x/R}{\sqrt{\tau}}) + erf(\frac{1 + x/R}{\sqrt{\tau}})]\tau = 4D_{LL}t_{rk}/R^2 D_{LL} = D_0 L^n, \tag{12.10}$$

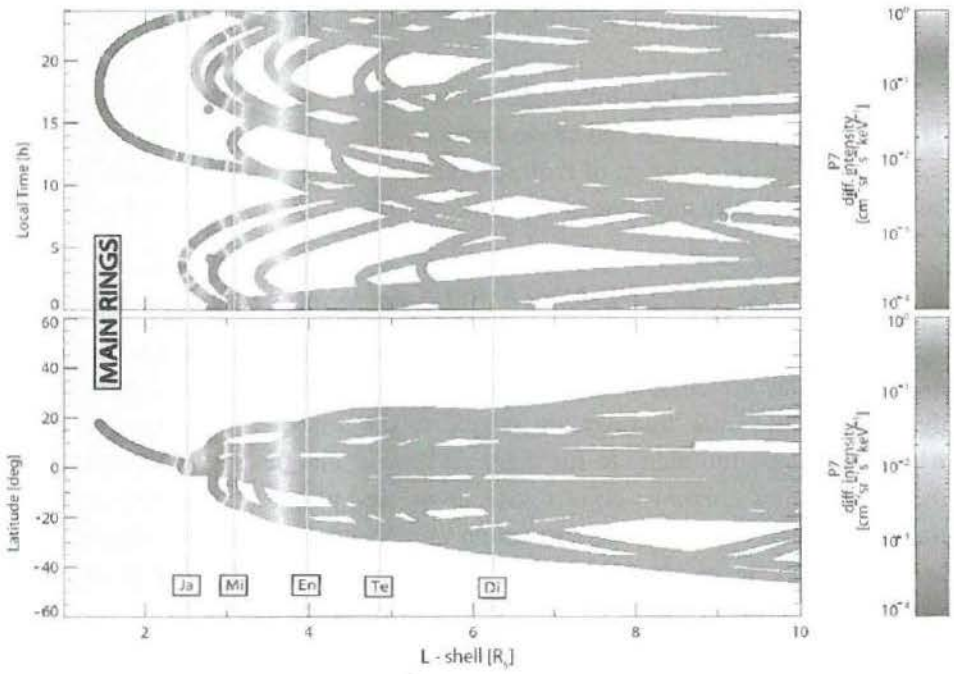

Fig. 12.13 Macrosignatures of energetic ions in the inner magnetosphere of Saturn as a function of L-shell and either local time (upper panel) or latitude (lower panel). Color-coded are the differential intensities of ions (> 10 MeV/nucleon) as measured between 2004 and 2007 by the Low Energy Magnetospheric Measurement System LEMMS onboard the Cassini spacecraft. (From Roussos, 2008.) A black and white version of this figure will appear in some formats. For the color version, please refer to the plate section.

with t_{rk} being the time an electron needs to travel through the absorption region, D_{LL} is the radial diffusion coefficient, R is the radius of the object causing the absorption. Therefore it is possible to calculate radial diffusion coefficients by studying the absorption signature profiles as a function of azimuthal separation from the object at the appropriate radial position, the magnetic flux shell or L-shell, connected to the object. By studying the same processes at different objects (or at different L-shells) a radial diffusion coefficient D_{LL} as a function of distance (or L-shell) can be determined as indicated in Fig. 12.14 from Roussos *et al.* (2007, 2008).

The same method was used to discover a neutral gas torus around the orbit of the Jovian moon Europa (Lagg *et al.*, 2003) or to identify new ring arcs (Roussos *et al.*, 2008), and to discover an additional noon-midnight electric field in Saturn's magnetosphere (Andriopoulou *et al.*, 2012).

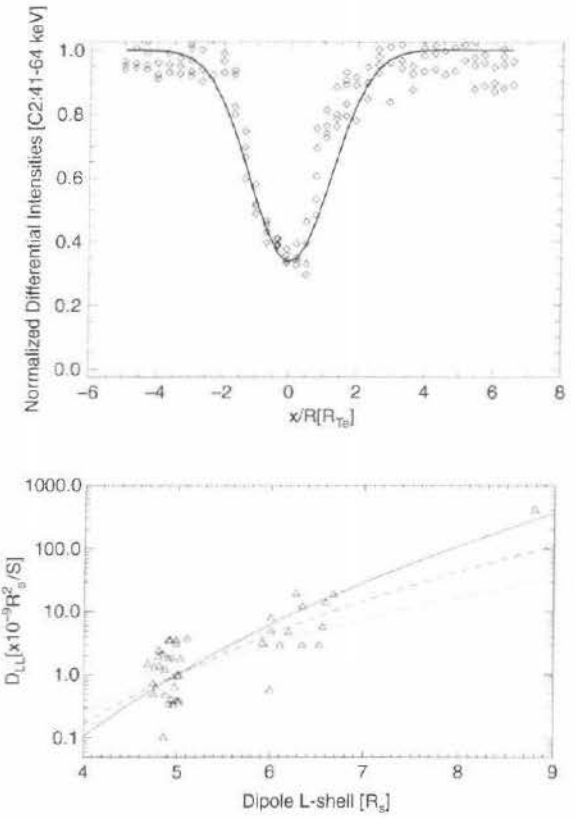

Fig. 12.14 Top: the symbols are the microsignature of Saturn's moon Tethys, the solid curve is the best fit. Bottom: L-dependence of radial diffusion coefficient D_{LL}. (From Roussos *et al.*, 2007.)

12.2.2.2 Determination of flow velocities

Another very important quantity that can be derived from energetic particle distributions is the calculation of particle flow velocities. Using the directional information and energy spectra from energetic-particle measurements it is possible to derive the particle anisotropies (Krupp *et al.*, 2001). Under the assumption that the anisotropy A_F is mainly due to flow and with the assumption that the energy spectrum can be described by a power law with exponent γ the flow velocities can be determined as

$$v_F = \frac{A_F v_{ion}}{2(\gamma + 1)}, \tag{12.11}$$

with v_{ion} being the particle velocity. As an example the derived global flow patterns in Jupiter's equatorial plane are shown in Fig. 12.15 as derived from energetic-particle measurements onboard the Galileo spacecraft. With these measurements it

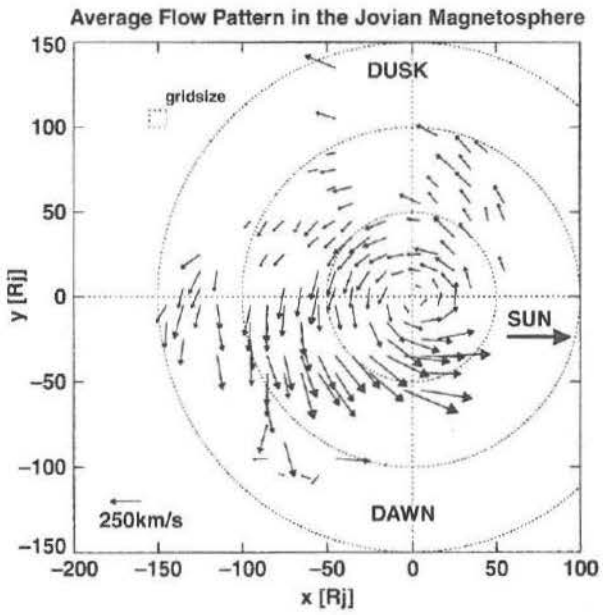

Fig. 12.15 Global flow patterns around Jupiter as derived from *Galileo* energetic particle measurements binned in $10 \times 10\ R_J$ bins. (From Woch *et al.*, 2004.)

is clear that plasma and energetic particles (sub-)co-rotate with the planet and that a strong dawn–dusk asymmetry in the flow patterns exists.

12.2.2.3 Determination of open–closed field-line boundaries

Another application of energetic particle distributions as a tool to investigate key magnetospheric regions is the determination of the boundary between open and closed field lines in the auroral zones of the Earth or Saturn. The principle is quite simple and requires only a good pitch angle coverage of the particle sensor, making it able to measure charged particles at a particular energy, but at both directions parallel and anti-parallel to the local magnetic field. Knowing that energetic particles bounce along closed field lines between their mirror points the expectation is that the ratio of particles with pitch angle 0 and 180 degrees is close to unity if the field lines are closed and substantially differ from unity if the spacecraft was connected to an open field line. Monitoring this ratio as a function of time therefore is used to determine the open–closed field-line boundary. An example from measurements inside Saturn's magnetosphere is shown in Fig. 12.16.

Marked in yellow is the section where the ratio between the two opposite channels parallel and anti-parallel to the local magnetic-field direction are very different, and an indication of open field lines. In the cases of Earth and Saturn, this boundary is related to the region in the plane's ionosphere of the main auroral oval.

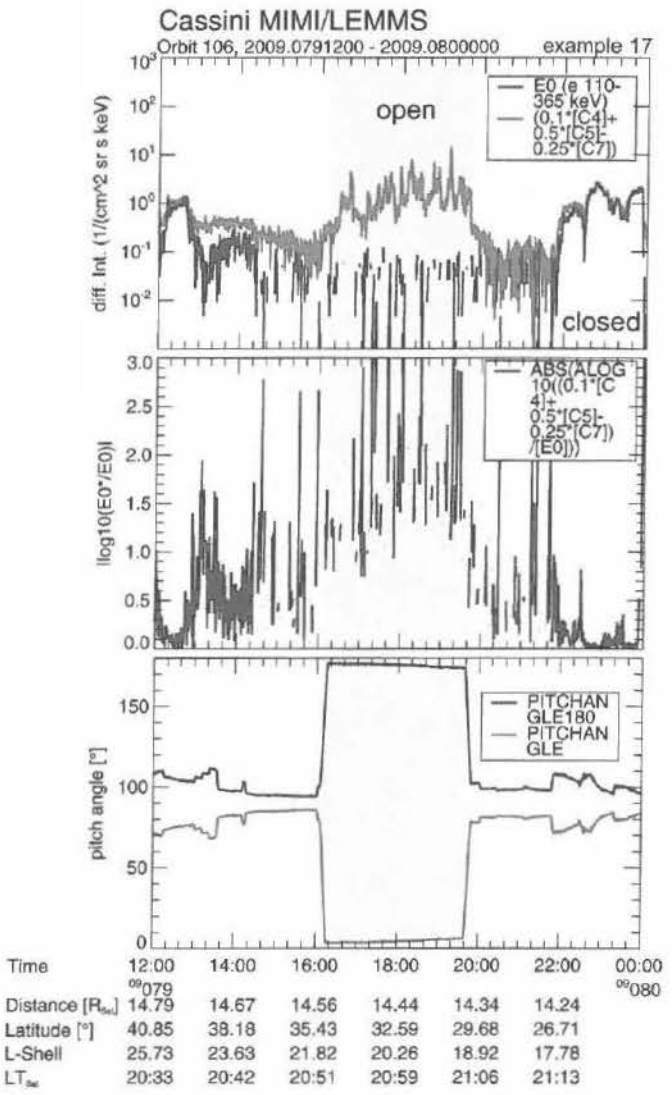

Fig. 12.16 Intensity of electrons along and against the magnetic-field direction inside Saturn's magnetosphere. A black and white version of this figure will appear in some formats. For the color version, please refer to the plate section.

12.3 Summary

In this chapter we have revisited the topic of energetic particles originating from the Sun and in planetary magnetospheres have been revisited. Covering energies up to hundreds of MeV energetic particle characteristics (energy spectra, directional information, intensities, ion composition, etc.) can be used to investigate acceleration mechanisms as well as global configuration and dynamics both in the

interplanetary space and inside planetary magnetospheres. They can be used as a tool to study plasma parameters nearly impossible to measure otherwise. Knowing their characteristics in our local environment in our solar system (distribution functions, sources and sinks, etc.) can help to better understand in general astrophysical phenomena within and outside our galaxy.